Phase Motion in the Scalar Low-Mass $\pi\pi$ Amplitude in $D^+ \to \pi^-\pi^+\pi^+$ Decay

Ignacio Bediaga and Jussara M. de Miranda
Centro Brasileiro de Pesquisas Físicas,
Rua Xavier Sigaud 150, 22290-180 – Rio de Janeiro, RJ, Brazil
bediaga@cbpf.br and jussara@cbpf.br

February 7, 2008

Abstract

Applying the Amplitude Difference method to Fermilab experiment E791 $D^+ \to \pi^-\pi^+\pi^+$ data, we measure the low mass $\pi^+\pi^-$ phase motion. Our results suggest a significant phase variation, compatible with the existence of an isoscalar $\sigma(500)$ meson, as previously reported using an isobar model fit to the full Dalitz-plot density.

Submitted to Physics Letters B
Keywords: Heavy Meson Decays; Dalitz-plot; Scalar Mesons; Resonances.
PACS Numbers: 13.25.Ft, 14.40.Ev, 14.40.Cs,11.80.Et.

Recently we proposed the isobar-based Amplitude Difference (AD) method to extract the phase motion of a complex amplitude in three-body heavy-meson decays [1]. With this method, the phase variation of a generic complex amplitude can be directly revealed through interference in the Dalitz-plot region where it crosses a well established resonant state, used as a probe. As a test, this method was successfully applied to data [2] to extract the well known phase motion of the scalar amplitude $f_0(980)$ observed in $D_s^+ \to \pi^-\pi^+\pi^+$ [1] decay. In the present paper we use the same method to study the low $\pi^+\pi^-$ mass region of the $D^+ \to \pi^-\pi^+\pi^+$ decay where Fermilab experiment E791 showed evidence for the existence of a light and broad scalar resonance [3].

To obtain good fit quality in a full Dalitz-plot analysis, E791 found it necessary to include an extra scalar particle, in addition to the well-established di-pion resonances [4]. For this new scalar state, parameterized as an S-wave Breit-Wigner resonance, they measured a mass and a width of $478^{+24}_{-23} \pm 17$ MeV/c^2 and $324^{+42}_{-40} \pm 21$ MeV/c^2, respectively. These parameters are compatible with those expected for the isoscalar meson $\sigma(500)$. The $D^+ \to \sigma(500)\pi^+$[3] decay appeared as the dominant contribution, accounting for approximately half the $D^+ \to \pi^-\pi^+\pi^+$ decays.

The E791 result has been widely discussed [5]-[10] and new data has become available [11]. However it is desirable to be able to confirm the result through a direct observation of the phase motion expected for a resonance [6, 7, 8]. In this context we apply the AD method to the low $\pi^+\pi^-$ mass region of the $D^+ \to \pi^-\pi^+\pi^+$ decay. We also compare the phase variation of the Breit-Wigner function found in the isobar Dalitz-plot analysis [3] to the model-independent method of this paper.

The present study is a reanalysis of the Fermilab experiment E791 data. Here we investigate a subset of the total phase space used by the experiment in their full Dalitz-plot analysis. A description of the experiment, data selection criteria, background parametrization and detector acceptance are found in references [3, 12]. The final $\pi^-\pi^+\pi^+$ invariant mass distribution is shown in Fig. 1. There are 1686 events with invariant mass between 1.85 and 1.89 GeV/c^2 shown in the shaded region of Fig. 1. The integrated signal-to-background ratio in this range is about 2:1. Fig. 2 shows the folded Dalitz-plot. The horizontal and vertical axes are the squares of the $\pi^+\pi^-$ invariant mass high (s_{12}) and low (s_{13}) combinations. The analysis presented here uses the hatched area of Fig. 2. We estimate 60 background events in a total of 197 candidate events. The background does not show any dependence on the s_{12} variable [3].

The detector acceptance in this region is almost constant. There is a very mild slope in the s_{13} acceptance, but no variation with s_{12}. Nevertheless the acceptance is taken into account to correct the event distributions shown later.

There are two conditions necessary to extract the phase motion of a generic am-

[1] Charge conjugate states are implied throughout the paper.

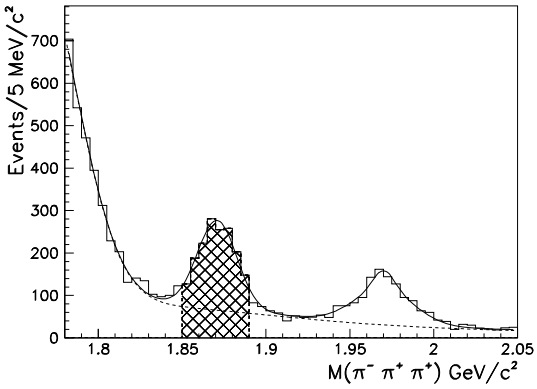

Figure 1: The $\pi^-\pi^+\pi^+$ invariant mass spectrum. The dashed line represents the total background. Events used for the D^+ isobar Dalitz-plot analysis [3] and in this AD method analysis are in the hatched area.

plitude with the AD method:

- A crossing region between the amplitude under study and a probe resonance has to be dominated by these two contributions.
- The integrated amplitude of the probe resonance must be symmetric with respect to an effective mass squared (m^2_{eff}). [2]

To study the low mass region in s_{13}, three well known resonances could serve as a probe in s_{12} in the $D^+ \to \pi^-\pi^+\pi^+$ decay: $\rho(770)$, $f_0(980)$ and $f_2(1270)$. However the broad $\rho(770)$ and $f_0(980)$ are too close to each other to pass the isolation criteria mentioned above, as can be seen in Fig. 2. On the other hand, the tensor $f_2(1270)$, $m_0^2 = 1.61$ GeV$^2/c^4$, is located where the $\rho(770)$ reaches a minimum due to its decay angular distribution in the crossed (s_{13}) channel, (see Fig. 3). In the $D^+ \to \pi^-\pi^+\pi^+$ decay, the $f_2(1270)$ contribution satisfies the necessary conditions of having a substantial contribution crossing the low mass region, this being the regions where all other amplitudes can be considered negligible. In particular, we estimate a contamination of 5% of $\rho(770)\pi^+$ events in the region of interest.

We assume that the only contributions in this region are the $f_2(1270)$ amplitude in s_{12} and the $\pi\pi$ complex amplitude under study in s_{13}. We write:

$$\begin{aligned}\mathcal{A}(s_{12}, s_{13}) \approx a_R \;\; & \mathcal{BW}_{f_2(1270)}(s_{12}) \;\; {}^{J=2}\mathcal{M}_{f_2(1270)}(s_{12}, s_{13}) + \\ & + \;\; a_s/(p^*/\sqrt{s}_{13}) \;\; sin\delta(s_{13}) \;\; e^{i(\delta(s_{13})+\gamma)},\end{aligned} \tag{1}$$

[2] An analysis with more amplitudes in a limited phase space could be done, but in a model dependent way.

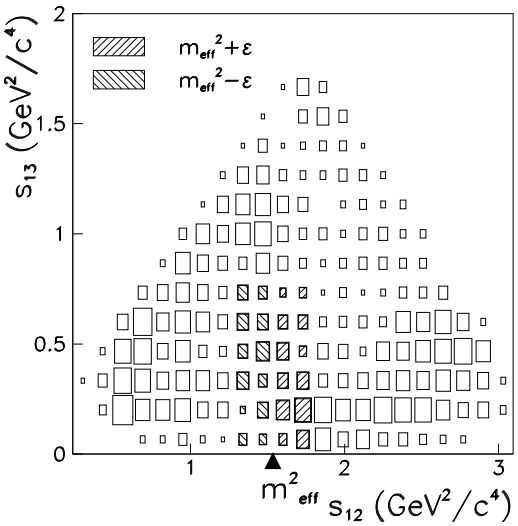

Figure 2: The folded $D^+ \to \pi^-\pi^+\pi^+$ Dalitz-plot distribution of the events in the hatched area of Figure 1. The events used by the AD method analysis are in the hatched region of this folded Dalitz-plot. The size of the area of each bin in the plot corresponds to the number of events in that bin.

where γ is the overall relative phase-difference between the two amplitudes (assumed to be constant and arising from both production and final-state-interaction (FSI) between the di-pion system and the bachelor pion); $sin\delta(s_{13})e^{i\delta(s_{13})}$ represents the most general amplitude for a two-body elastic scattering, $p^*/\sqrt{s}_{13}$ is a phase space integration factor to make this description compatible with $\pi\pi$ scattering and p^* is the pion momentum measured in the resonance rest frame; ${}^{J=2}\mathcal{M}_{f_2(1270)}(s_{12}, s_{13})$ is the angular function for the $f_2(1270)$ tensor resonance given by $\frac{4}{3}(\mid \mathbf{p_3} \mid\mid \mathbf{p_2} \mid)^2(3cos^2\theta - 1)$, θ being the angle between the pions 2 and 3, and J the angular momentum of the resonance; and a_R and a_s are the production strengths. The AD method assumes that the $\pi^+\pi^-$ production is constant over the effective mass range considered and a_R and a_s are energy independent. Finally the Breit-Wigner distribution is given by:

$$\mathcal{BW} = \frac{m_0\Gamma_0}{m_0^2 - s - im_0\Gamma(s)}. \tag{2}$$

The width is given by $\Gamma(s) = \Gamma_0\frac{m_0}{m}\left(\frac{p^*}{p_0^*}\right)^{2J+1}\frac{{}^JF^2(p^*)}{{}^JF^2(p_0^*)}$, where the central barrier factor is ${}^{J=2}F = 1/\sqrt{9 + 3(rp^*)^2 + (rp^*)^4}$. The parameter r is the radius of the resonance ($\sim 3fm$)[13] and $p^* = p^*(m)$ is the momentum of decay particles at mass m, measured in the resonance rest frame, $p_0^* = p^*(m_0)$, where m_0 is the resonance mass.

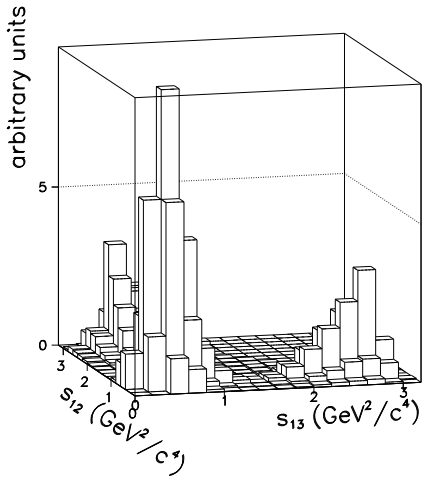

Figure 3: Fast MC $\rho(770)\pi$ Dalitz-plot distribution in $D^+ \to \pi^-\pi^+\pi^+$ decay.

Both $\Gamma(s)$ and the angular function ${}^{J=2}\mathcal{M}_{f_2(1270)}$ for the $f_2(1270)$ resonance produce asymmetries in the s_{12} distribution. We use a $D^+ \to f_2(1270)\pi^+$ fast Monte Carlo (MC) simulation[3] to study the behavior of the probe resonance distribution in the s_{12} and s_{13} variables. The event distribution for $f_2(1270)$ in the s_{12} subsystem from Monte Carlo is shown in Fig. 4. We choose an effective square mass of 1.535 GeV$^2/c^4$ such that the number of events between m^2_{eff} and $m^2_{eff} + \epsilon$ ($\epsilon = 0.26$ GeV$^2/c^4$) is equal to the number of events integrated between m^2_{eff} and $m^2_{eff} - \epsilon$.

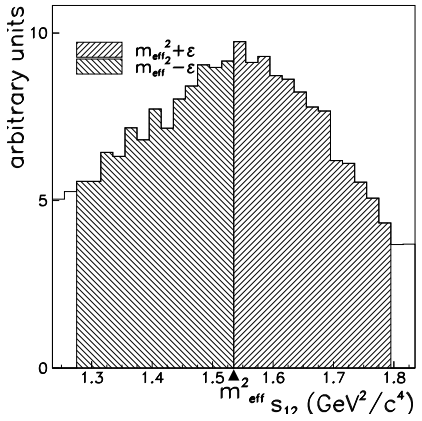

Figure 4: Fast MC simulation$f_2(1270)$ s_{12} distribution, divided into $m_0^2+\epsilon$ and $m_0^2-\epsilon$, integrated between the threshold and 0.8 GeV^2 in s_{13}.

[3]The Monte Carlo events are generated according to the physical amplitude squared using a uniform phase space density and weighted by the detector acceptance distribution over the Dalitz-plot.

For events in s_{12} between m^2_{eff} and $m^2_{eff}+\epsilon$ in s_{12}, ${}^{J=2}\mathcal{M}_{f_2(1270)}(s_{13})$ is shown in Fig. 5a and for those between m^2_{eff} and $m^2_{eff}-\epsilon$ in Fig. 5b[4]. We can see that these two plots are just slightly different. In our analysis we consider the approximation ${}^{J=2}\mathcal{M}^{+}_{f_2(1270)}(s_{13}) \approx {}^{J=2}\mathcal{M}^{-}_{f_2(1270)}(s_{13})$ and take the average function ${}^{J=2}\bar{\mathcal{M}}_{f_2(1270)}(s_{13})$. An important effect that we have to take into account is the zero of this function at $s_{13}\sim$0.48 GeV$^2/c^4$. Below we discuss the consequences of that for this AD method application.

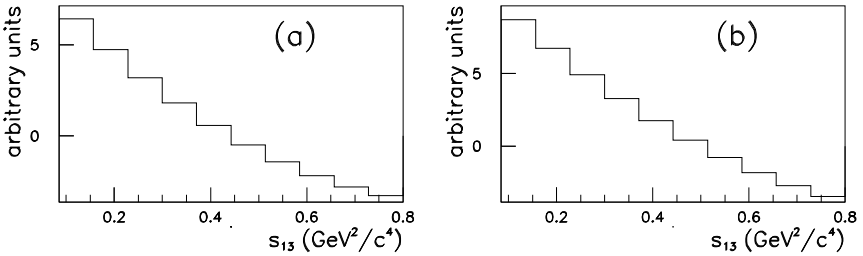

Figure 5: Fast MC of angular distribution function alone, ${}^{J=2}\mathcal{M}_{f_2(1270)}$, in s_{13} for (a) events between m^2_{eff} and $m^2_{eff}+\epsilon$ and (b) events between m^2_{eff} and $m^2_{eff}-\epsilon$.

To be brief, from here on we use ${}^{J=2}\bar{\mathcal{M}}_{f_2(1270)}(s_{13}) = \bar{\mathcal{M}}$ and $p^*/\sqrt{s}_{13} = p'$. The main equation of the AD method applied to the integrated amplitude-square difference is [1, 2]:

$$p'/\bar{\mathcal{M}}(\Delta\int\mathcal{A}^2) = p'/\bar{\mathcal{M}}(\int_{m^2_{eff}}^{m^2_{eff}+\epsilon} \mid \mathcal{A}(s_{12},s_{13}) \mid^2 ds_{12} - \int_{m^2_{eff}-\epsilon}^{m^2_{eff}} \mid \mathcal{A}(s_{12},s_{13}) \mid^2 ds_{12})$$
$$\approx -\mathcal{C}(sin(2\delta(s_{13})+\gamma) - sin\gamma), \qquad (3)$$

where $\mathcal{C}$ is an overall constant.

From Eq. 2, it follows that the function $\Delta\int\mathcal{A}^2p'/\bar{\mathcal{M}}$ directly reflects the behavior of $\delta(s_{13})$. A constant $\Delta\int\mathcal{A}^2p'/\bar{\mathcal{M}}$ implies a constant $\delta(s_{13})$ which is the case for a non-resonant contribution. In the same way, a slow phase motion will produce a slowly varying $\Delta\int\mathcal{A}^2p'/\bar{\mathcal{M}}$ distribution, and a full resonance phase motion produces a clear signature in $\Delta\int\mathcal{A}^2p'/\bar{\mathcal{M}}$ with the presence of zero, maximum and minimum values.

[4]The plots were produced by a fast MC of the angular distribution function alone, with no detector influence included. We represent this function with the same binning used for our data events.

As mentioned previously, the background has no dependence on s_{12} and its contribution vanishes from the $\Delta \int \mathcal{A}^2$ distribution. The $\int \mathcal{A}^2$ in s_{13} for events integrated in s_{12} m^2_{eff} and $m^2_{eff} + \epsilon$ and m^2_{eff} and $m^2_{eff} - \epsilon$, corrected by the acceptance shape, are presented in Figs. 6a and 6b, respectively; these events correspond to the hatched area of Fig. 2. We obtain $\Delta \int \mathcal{A}^2$ shown in histogram 6c, by subtracting the 6b histogram from that in 6a.

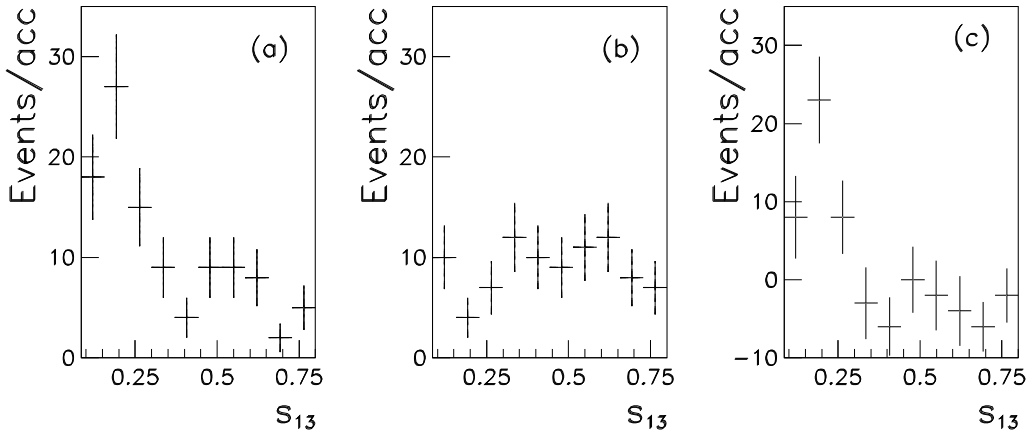

Figure 6: Event distributions projected onto the s_{13} axis (a) for all events in the s_{12} interval $\int_{m_0^2}^{m_0^2+\epsilon} \mid \mathcal{A}(s_{12}, s_{13}) \mid^2 ds_{12}$, and (b) for events $\int_{m_0^2-\epsilon}^{m_0^2} \mid \mathcal{A}(s_{12}, s_{13}) \mid^2 ds_{12}$. The distributions are acceptance corrected such that the overall data statistics is conserved. Plot (c) shows the $\Delta \int \mathcal{A}^2$ distribution .

To extract the phase motion, we divide $\Delta \int \mathcal{A}^2$ (Fig. 6c) by $\bar{\mathcal{M}}$ (average of the distributions in Figs. 5a and b), and multiply by p', both known functions of s_{13}. Then the only s_{13} dependence of the right hand side of Eq. 2 is in the phase motion $\delta(s_{13})$. From Fig. 5, the zero at $s_{13} \sim 0.48$ GeV$^2/c^4$ in the angular function, produces a singularity around this value in $\Delta \int \mathcal{A}^2 p'/\bar{\mathcal{M}}$. In Fig. 7 we show the $\Delta \int \mathcal{A}^2 p'/\bar{\mathcal{M}}$ distribution. To treat the effect of the singularity, we have used a binning such that the singularity is placed in the middle of one bin. Doing this, we isolate the singularity in a single bin (bin 6) and discard it in the analysis. We point out that the location of this singularity can only affect the exact position of the minimum of $\Delta \int \mathcal{A}^2 p'/\bar{\mathcal{M}}$. It does not change the general features observed, in Fig. 7, that this quantity starts at zero, has maximum and minimum values, and comes back to zero, the signature for a strong phase variation. The confidence level for a straight line fit to the data in Fig. 7 is 4.6%, while the separation between the maximum and

minimum values has a significance level of 2.6 r.m.s.

We can see that the 6^{th} bin has a huge error, which corresponds to the bin due to the presence of the singularity.

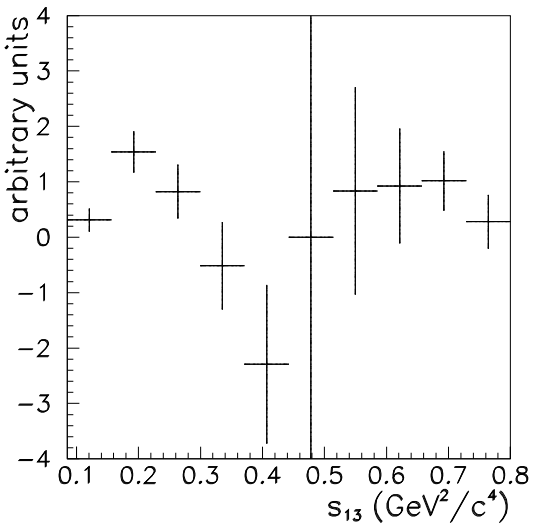

Figure 7: The distribution of $\Delta \int \mathcal{A}^2\, p'/\bar{\mathcal{M}}$ in s_{13}. Note that the scale is arbitrary once the data, $\Delta \int \mathcal{A}^2$, is multiplied by an unnormalized function $p'/\bar{\mathcal{M}}$. The error bars represent statistical errors only.

Assuming that $\delta(s_{13})$ is an analytical function of s_{13}, Eq. 2 allows us to set the two following conditions at the maximum and minimum values of $\Delta \int \mathcal{A}^2 p'/\bar{\mathcal{M}}$, respectively.

$$(\Delta \int \mathcal{A}^2) p'/\bar{\mathcal{M}}_{max} \rightarrow sin(2\delta(s_{13}) + \gamma) = -1 \tag{4}$$

and

$$(\Delta \int \mathcal{A}^2) p'/\bar{\mathcal{M}}_{min} \rightarrow sin(2\delta(s_{13}) + \gamma) = 1. \tag{5}$$

With these two conditions, we obtain γ and $\mathcal{C}$, and with these values we can extract directly $\delta(s_{13})$ from Fig. 7 by inverting Eq. 2.

To propagate the statistical errors from Fig. 6 to the values of the γ and $\delta(s_{13})$, we "produce" statistically compatible "experiments" by allowing each bin of Fig. 6a and Fig. 6b to fluctuate randomly following a Poisson law. We then solve the problem for each set. The statistical error in each bin for $\delta(s_{13})$ is the r.m.s. of the $\delta(s_{13})$ distributions from the Monte Carlo experiments. For the systematic errors, we change the ϵ parameter ($\epsilon = 0.22$ GeV$^2/c^4$ and $\epsilon = 0.30$ GeV$^2/c^4$); we examine the possible influence of other neglected amplitudes contributing in this region of the phase

space (based on the E791 amplitude measurements for non-resonant, $f_0(1370)\pi^+$ and $\rho^0(1450)\pi^+$[3] contributions); and, to study the effect of averaging ${}^{J=2}\bar{\mathcal{M}}_{f_2(1270)}(s_{13})$ distributions, we use each distribution of Fig. 5a and Fig. 5b separately. The three systematic errors, while treated separately bin-by-bin, are found to be of an average size, relative to the statistical uncertainty, of 1, 0.6, and 0.4, respectively. They are added in quadrature.

We measure $\gamma = 3.31 \pm 0.33 \pm 0.49$ (with the first error statistical and the second systematic)[5]. The value is somewhat larger than the E791 full Dalitz-plot analysis value ($\gamma_{Dalitz} = 2.59 \pm 0.19$) [3]. The asymmetry of the distribution in Fig. 4 and the consequent use of an effective mass-squared for the $f_2(1270) = 1.535$ GeV$^2/c^4$ instead of the nominal mass is responsible for the observed shift. To evaluate the magnitude of this effect, we generated 1000 fast MC samples with only two amplitudes, $f_2(1270)$ and $\sigma(500)$. For both, we used Breit-Wigner functions with the E791 parameters, including the phase-difference of 2.59 rad. We extract γ from these 1000 samples with the method presented here. The result has a mean value of 3.07 $\pm$ 0.10 rad, instead of the input value 2.59 rad. We estimate an offset of -0.48 (2.59 - 3.07) for γ from the difference between the generated and measured values in this Monte Carlo test. This yields to a corrected $\gamma_{corr} = 2.83 \pm 0.38 \pm 0.49$. The production phase-difference between the $f_2(1270)\pi^+$ and the $\sigma(500)\pi^+$ decays of D^+ measured in the isobar Dalitz analysis is in good agreement with γ_{corr} from the AD method.

With our γ and $\mathcal{C}$ values we solve Eq. 2 for $\delta(s_{13})$ for each s_{13} bin. However, there are ambiguities that arise due to the sin^{-1} operations. Table 1 shows the four possible solutions for $\delta(s_{13})$[6]. To resolve the ambiguities we use the assumption that the phase is zero at threshold and is an increasing, monotonic, and smooth function of s_{13}.

The solution, after the above criteria for $\delta(s_{13})$, including systematic and statistical errors, is shown in Fig. 8 and in bold values in Table 1. We see a strong phase variation of about 180^0, starting at threshold and saturating around $s_{13} = 0.6$ GeV$^2/c^4$. The limited sample size does not allow us to perform an accurate measurement of the mass and width parameters of a BW resonance fitted to this plot. We can only say that, at least for the preferred solution, the phase variation is compatible with the complete phase motion through 180^0 expected for a resonance. This result is in

[5]Here, in addition to the systematic error sources mentioned above, we have also incorporated one related to the binning choice that we made to avoid the singularity in $\bar{\mathcal{M}}$. If we change the binning such that the singularity is placed between bins we measure $\gamma = 3.52 \pm 0.53$.

[6]The occurrence of two different sets of statistical errors in $\delta(s_{13})$ is caused by convolution of the error in γ and in $\Delta \int \mathcal{A}^2$, and the fact that the distributions of those variables are not symmetrical. Moreover, the method naturally favors $\delta(s_{13})$ values coming from the maximum and minimum bins in Figure 7, since these are used to determine the C and γ that are in turn used to determine all $\delta(s_{13})$ values. The uncertainties are therefore relatively smaller in these two bins than in the other bins, a result that may be attributed in part to the model itself rather than the quality of the data in these bins.

bin	$\Delta \int \mathcal{A}^2\, p'/\mathcal{M}$	$\delta_0(s_{13})(^\circ)$	$\delta_1(s_{13})(^\circ)$	$\delta_2(s_{13})(^\circ)$	$\delta_3(s_{13})(^\circ)$	systematic($^\circ$)
1	0.27 ± 0.18	-104 ± 20	76 ± 20	$\mathbf{7 \pm 8}$	187 ± 8	**17**
2	1.31 ± 0.32	-139 ± 15	$\mathbf{42 \pm 15}$	$\mathbf{42 \pm 12}$	222 ± 12	**20**
3	0.74 ± 0.43	-110 ± 21	$\mathbf{70 \pm 21}$	13 ± 13	193 ± 13	**39**
4	-0.46 ± 0.71	-90 ± 26	$\mathbf{91 \pm 26}$	-8 ± 16	173 ± 16	**23**
5	-2.1 ± 1.3	-49 ± 16	$\mathbf{132 \pm 16}$	-49 ± 21	$\mathbf{132 \pm 21}$	**11**
7	0.8 ± 1.8	-109 ± 27	71 ± 27	12 ± 25	$\mathbf{192 \pm 25}$	**27**
8	0.91 ± 1.01	-110 ± 23	70 ± 23	13 ± 17	$\mathbf{193 \pm 17}$	**11**
9	0.97 ± 0.51	-112 ± 20	68 ± 20	15 ± 10	$\mathbf{195 \pm 10}$	**13**
10	0.28 ± 0.49	-101 ± 22	79 ± 22	4 ± 10	$\mathbf{184 \pm 10}$	**5**

Table 1: Second column are the $\Delta \int \mathcal{A}^2\, p'/\bar{\mathcal{M}}$ values plotted in Fig.7; note the arbitrary normalization. Columns 3 to 6 are four possible solutions for $\delta(s_{13})$: $\delta_0(s_{13})$ for $(2\delta(s_{13}) + \gamma)$, $\delta_1(s_{13})$ for $(2\delta(s_{13}) + \gamma) + 2\pi$, $\delta_2(s_{13})$ for $\pi - (2\delta(s_{13}) + \gamma))$ and $\delta_3(s_{13})$ for $\pi - (2\delta(s_{13}) + \gamma)) + 2\pi)$. The systematic errors are described in the text.

agreement with the evidence for a broad and low mass scalar resonance suggested by the previous E791 result using the full Dalitz-plot analysis [3].

The Breit-Wigner phase motion for the E791 mass and width parameters, combined with other scalar contributions obtained from that fit [3], is shown as the continuous line of Fig. 8. We can see a two standard deviation difference at lowest and highest $\pi^+\pi^-$ invariant masses squared, in opposite directions, but in overall agreement with the mass region where a scalar meson σ must have its strong phase variation. Both results, the E791 with a Breit-Wigner phase variation, and the one presented in this paper, show a stronger phase variation than that obtained with theoretical constraints in $\pi\pi \to \pi\pi$ elastic scattering data in the scalar-isoscalar channel below 1 GeV [9, 14, 15]. The discrepancy between these results could be an indication that applying Watson's theorem [16] is not straight-forward when comparing the phase motion of a two-body elastic interaction to the three-body decays.

We have presented an extraction of the phase motion of the low mass $\pi^+\pi^-$ scalar amplitude using the well known $f_2(1270)$ tensor meson in the crossing channel acting as an interferometer. The result is obtained with an event counting procedure in a region of the phase space which is dominated by a D-wave $f_2(1270)$ interfering with the S-wave. The derivation of the phase motion relies heavily on the assumption that the maximum and minimum bins in Fig. 7 correspond to the quantity $S = sin(2\delta + \gamma) = +1$ and -1. The clear presence of a maximum and a minimum, separated from each other by 2.6 standard deviations, supports this assumption. Given this caveat, the solution for $\delta(s_{13})$ has a variation of about 180^0, consistent with a resonant $\sigma(500)$ contribution. We also obtain good agreement between the FSI γ_{corr} determined with the AD method and the γ observed in the full Dalitz-plot analysis using an isobar model [3]. These results support the previous evidence for an important contribution

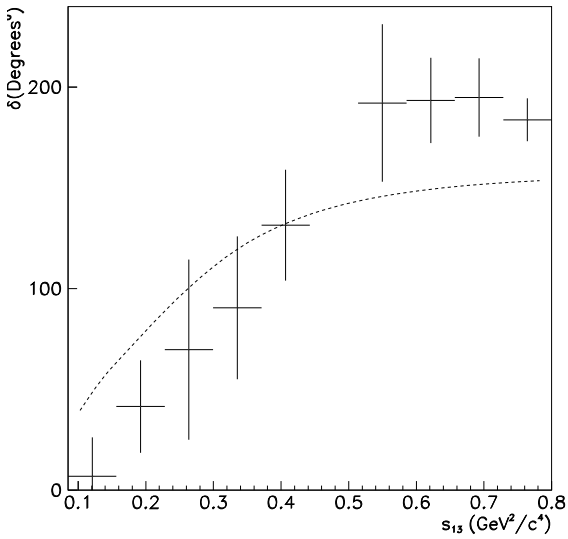

Figure 8: The phase values $\delta(s_{13})$ from our preferred solution versus the invariant $\pi^+\pi^-$ mass squared with statistical and systematic errors added in quadrature. The continuous line is the Breit-Wigner phase motion with the E791 parameters for the $\sigma(500)$[3].

of the isoscalar $\sigma(500)$ meson in the $D^+ \to \pi^-\pi^+\pi^+$ decay [3].

Acknowledgement

We would like to acknowledge the E791 Collaboration for allowing us to use their data for this paper and for the valuable discussions. We would like to thank Profs. Jeff Appel, Steve Bracker, Hans Günter Dosch, Brian Meadows, Wolfgang Ochs, and Alberto Reis for suggestions and important comments.

References

[1] I. Bediaga and J. Miranda, Phys. Lett. **B550** (2002) 135.

[2] I. Bediaga for E791 Collaboration, proceedings of Scalar Meson Workshop, SUNYIT, Utica, NY, May 2003 and hep-ex/0307008.

[3] E791 Collaboration, E. M. Aitala *et al.*, Phys. Rev. Lett. **86** (2001) 770.

[4] Particle Data Group, Hagiwara *et al.*, Phys. Rev. **D66** (2002) 010001.

[5] H. G. Dosch, E. M. Ferreira, F. S. Navarra, M. Nielsen, Phys. Rev. **D65** (2002) 114002; I. P. Cavalcante, J. Sa Borges, J. Phys. **G28** (2002) 1351; A. A. Natale, C. G. Roldao, J. P. V. Carneiro, Phys. Rev. **C65** (2002) 014902; R. Gatto, G. Nardulli, A. D. Polosa, N. A. Tornqvist, Phys. Lett. **B494** (2000) 168; C. Dib, R. Rosenfeld, Phys. Rev. **D63** (2001) 117501; A. Gomez Nicola, J. R. Pelaez, Phys. Rev. **D65** (2002) 054009; M. Ishida, proceedings of YITP - RCNP Workshop on Chiral Restoration in Nuclear Medium, Kyoto, Japan, 7-9 October 2002 and hep-ph/0212383; S. Bianco, F. L. Fabbri, D. Benson, I. Bigi, Riv. Nuovo Cim. **26N7** (2003) 1.

[6] F. E. Close and N. Törnqvist, J. Phys. **G28** (2002) 249.

[7] T. Barnes, proceedings of the HADRON2001 Conference Summary, Protvino, Russia, September 2001 and hep-ph/0202157.

[8] Peter Minkowski and Wolfgang Ochs, proceedings of QCD 2002 Euroconference, Montpellier, 2-9 July 2002. Nucl. Phys. **B121** (Proc. Suppl.) (2003) 119 and hep-ph/0209225.

[9] J. A. Oller, Phys. Rev. **D71** (2005) 054030.

[10] A. D. Polosa, proceedings of the 2nd Workshop on the CKM Unitarity Triangle, Durham, England, 5-9 April 2003 and hep-ph/0306298.

[11] CLEO Collaboration, H. Muramatsu *et al.*, Phys. Rev. Lett. **89** (2002) 251802; BES Collaboration,J. Bai *et al.*, Nucl. Phys. **28** (2004) 215 and hep-ex/0404016; Antonella Antonelli, proceedings of PIC 2002, Stanford, California, USA, June 2002 and hep-ex/0209069; BELLE Collaboration, K. Abe *et al.*, proceedings of XI International Symposium on Lepton and Photon Interactions at High Energies, Fermilab, 11-16 August 2003 and hep-ex/0308043; FOCUS collaboration, J. M. Link *et al.* Phys. Lett. **B585** (2004) 200.

[12] E791 Collaboration, E. M. Aitala *et al.*, Phys. Rev. Lett. **86** (2001) 765.

[13] ARGUS Collaboration, H. Albrecht *et al.*, Phys. Lett. **B308** (1993) 435.

[14] R. Kaminski, L. Lesniak, B. Loiseau, Phys. Lett. **B551** (2003) 241.

[15] C. Amsler, N. A. Törnqvist, Phys. Rep. **389** (2004) 61.

[16] K.M. Watson, Phys. Rev. **88** (1952) 1163.